Int. J. Electrochem. Sci., 13 **(2018)** 6522 – 6536, doi: 10.20.964/2018.07.50

International Journal of ELECTROCHEMICAL SCIENCE
www.electrochemsci.org

Synergistic Inhibition Effect of Sodium Tungstate and Zinc Sulphate on Mild Steel Corrosion in Seawater

Jinliang Zhang[1,2], *Lijing Zhang*[1,*], *Gang Tao*[1], *Fangying Cui*[3]

[1] College of Safety Science and Engineering, Nanjing Tech University, Nanjing 210009, China
[2] School of Materials and Chemical Engineering, Ningbo University of Technology, Ningbo 315211, China
[3] School of Chemistry and Chemical Engineering, Chongqing University, Chongqing 400044, China
[*]E-mail: zhanglj_njtech@163.com

Received: 8 March 2018 / *Accepted:* 3 May 2018 / *Published:* 5 June 2018

The desirable concentrations of sodium tungstate (ST) along with zinc sulfate (ZS) were selected for mild steel in seawater, and the inhibition effect of ST and ZS under wet/dry cyclic condition was investigated using weight loss and electrochemical methods. Results showed that the inhibition efficiency could reach 84.81% after 10 wet/dry cycles. Corrosion products were observed and analyzed by scanning electron microscopy (SEM) and X-ray diffraction (XRD). Corrosion behaviours under different wet/dry ratios were studied, which showed that the longer drying time was, the more serious corrosion was. The inhibition mechanism was that Fe_2WO_6 attached to the steel surface and retarded the corrosion reaction.

Keywords: Corrosion inhibition; Synergistic effect; Mild steel; EIS; Weight loss.

1. INTRODUCTION

Ocean cover 71% of the earth and the development of marine resources is one of the important means to solve the shortage of resources. However, seawater is a kind of typical electrolyte [1], which can etch and damage the engineering equipments that are serving in ocean [2-6]. Generally speaking, marine corrosion environment is divided into five zones: atmospheric zone, splash zone, tidal range zone, full immersion zone and sea mud area [7, 8]. The corrosion at splash zone is the most serious due to the high salt content [9], shock waves [10], dry-wet alternate [11], sufficient oxygen [12] and plenty of ultraviolet irradiation and so on. Various methods have been tried to avoid corrosion at splash zone [13-15] such as increasing the thickness of the steel plate, adding alloy elements [16], spraying anti-corrosion coatings [17] and coating protection. However, increasing steel plate thickness wastes

materials, and can't fundamentally solve the problem of corrosion. Adding alloy elements is also not the ideal method because alloy is expensive and may cause galvanic corrosion. As to protective coating, it is likely to appear bubble and peel due to the long-term impact of wave, causing severe local corrosion. Overlying strata protection methods such as metal hot spraying [18], hot dip plating [19] are limited for widely applying because of the expensive materials and complex operation. In view of the shortcomings of all the methods above, it is urgent to seek after an economic and effective corrosion protection method, which is simple and convenient to operate, so that to ensure steel structure facilities long-term and security service at splash zone.

Institute of Oceanology of Chinese Academy of Sciences succeeded in the research and development of Petrolatum tape cover (PTC), and the schematic is shown in Fig. 1. PTC is composed of petrolatum corrosion protective cream, petrolatum corrosion protective band, sealing buffer layer and corrosion protective cover. Petrolatum corrosion protective cream is the major anti-corrosion material, which is located in the innermost part of the PTC technology, closely contact with the protected structures. Its property affects the stability and durability of PTC. PTC technology has the following advantages: excellent adhesive property, low surface treatment requirement, simple construction craft, light quality, environmental friendly etc, which has been proved to be of high efficiency for steel corrosion prevention in splash zone [20]. The corrosion inhibitor is one of the important constituent parts of the petrolatum. Therefore, it makes sense to choose appropriate inhibitors so that PTC could be more efficient for protecting the steel structures away from corrosion. One of the characteristics of the splash zone is wet/dry alternate, so great importance was attached to the research of mild steel corrosion behaviour at wet/dry cyclic condition and the exploration of corrosion inhibitor that is suited to the complex corrosion environment. Sodium tungstate has been researched as steel corrosion inhibitor in many papers, which showed good inhibition effect when the concentration was appropriate [21-26]. In many cases, synergism between inhibitors could play better anticorrosive effects [27, 28]. Thus, focus is shifted to mixed inhibitors to take advantage of synergistic effect. In present study, sodium tungstate (ST, Na_2WO_4) along with zinc sulfate (ZS, $ZnSO_4$) were chosen for synergistic inhibition towards steel corrosion in the wet/dry cyclic experiments, which had never been explored before.

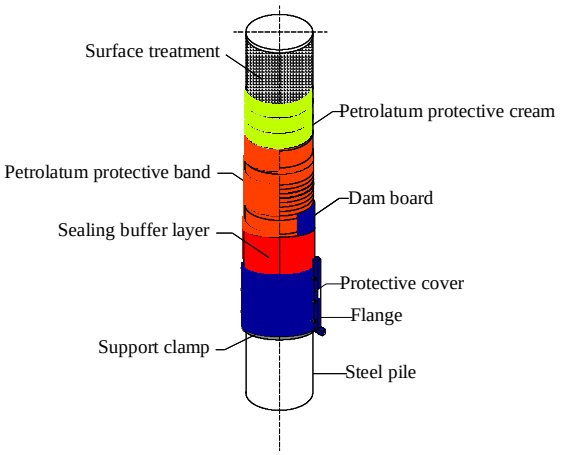

Figure 1. Schematic of PTC technology

2. EXPERIMENTAL

2.1. Materials

The experiments were performed with mild steel whose chemical composition (wt.%) was 0.16 C, 0.53 Mn, 0.30 Si, < 0.045 P, < 0.055 S, and Fe remainder. Samples of 50 × 20 × 5 mm size were used for weight loss tests, while that for electrochemical experiments were embedded in epoxy resin with an exposed area of 1 cm^2. Prior to measurement, the samples were polished with emery papers from 400 to 800 grade for weight loss tests and 400 to 2000 grade for electrochemical measurements. Then, the specimens were washed with distilled water, degreased with ethanol, and dried with a cold air blaster.

The aggressive solution: one is natural seawater from Huiquan Bay in Qingdao, the other is seawater that contained ST and ZS.

2.2. Wet/dry cyclic experiments

The specimens were immersed in and pulled out of the aggressive solution at a certain speed. In this work, one cycle includes immersing the specimens in solution with or without inhibitors for 12 h, then taking it out and drying at 298 K and 50% humidity for 12 h. The temperature and humidity were controlled by a thermostatic and humidistatic chamber. The solution was replaced every cycle, and 10 cycles were performed in the experiment.

2.3. Weight loss tests

Samples were weighed accurately before in a wet/dry cyclic state. After 10 cycles, samples were disposed with chemical methods as GB/T 16545-1996 described. After dried 24 h, samples were weighed again. Three parallel specimens were used to check the reproducibility.

2.4. Electrochemical measurements

A conventional three-electrode cell with a platinum foil of 2 × 2 cm as counter-electrode and a saturated calomel electrode (SCE) provided with the Luggin capillary as reference electrode was used for electrochemical measurements, which were conducted with Solartrom 1287~1260 electrochemical workstation. EIS was carried out in 100 kHz–10 mHz frequency range at the steady open circuit potential (OCP) disturbed with amplitude of 10 mV. The data were analyzed by ZSimpWin fitting software. EIS tests were conducted after immersing in the solution for one hour. The potentiodynamic polarization curves which were obtained from −250 mV to +250 mV (*vs.* OCP) with a scan rate of 1 mV s^{-1}, were conducted after 10 cycles. All the measurements were performed at 298K with a water bath controlling the temperature.

2.5. Corrosion product analysis

The surface morphology of the samples after 10 cycles in seawater with and without STZS was observed by the scanning electron microscopy (SEM) Hitachi S-3400N. Corrosion products were scraped off from the specimens that have been corroded using a razor blade, and were observed by X-ray diffraction (XRD), which were performed using the Rigaku-D/m ax2500PC.

3. RESULTS AND DISCUSSION

3.1. The selection of inhibitor concentration

3.1.1. Polarization measurements

Fig. 1 presents the potentiodynamic polarization curves of mild steel in seawater with various concentrations of Na_2WO_4 and mixed inhibitors contained 1.0 g/L Na_2WO_4 and different concentrations of $ZnSO_4$, respectively. Table 1 listed the electrochemical parameters, namely, the corrosion potential (E_{corr}), cathodic (anodic) tafel slopes β_c (β_a) and corrosion current density (I_{corr}).

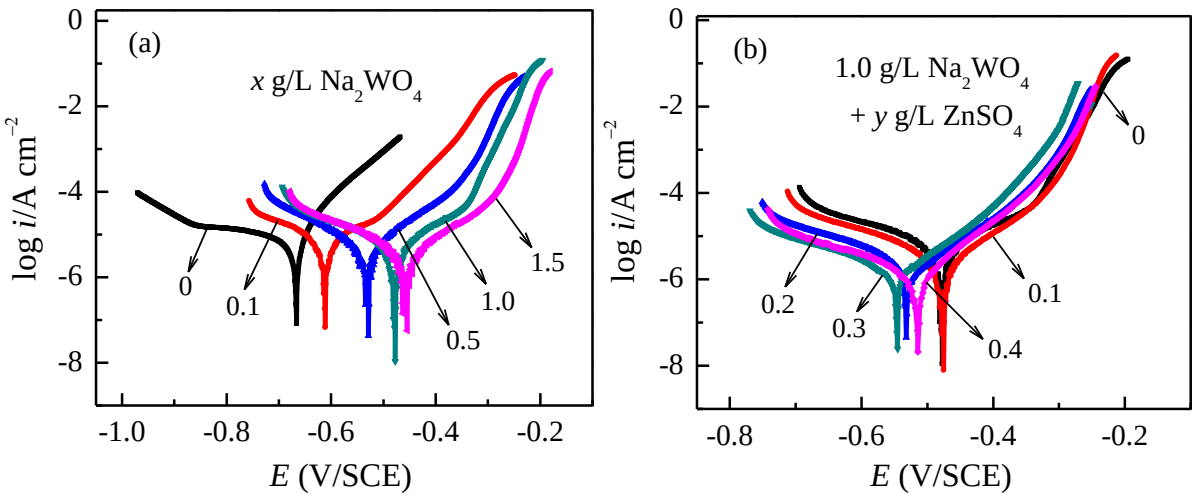

Figure 1. Potentiodynamic polarization curves of mild steel in seawater with (a) x (x = 0~1.5) g/L Na_2WO_4 and (b) 1.0 g/L Na_2WO_4 + y (y = 0~0.4) g/L $ZnSO_4$.

Fig. 1a showed that the shapes of cathodic polarization curves didn't change much after adding the inhibitor, which implied that the existence of the Na_2WO_4 had little effect on the cathode reaction mechanism. On the contrary, when it came to the anode polarization curves, an obvious change happened in shape, that is the curves shifted to lower current density region with the increase of Na_2WO_4 concentration, suggesting that anodic dissolution was retarded significantly. The phenomenon may caused by the WO_4^{2-} that dissociated from Na_2WO_4 adsorbing on the surface of steel and competing with the Cl^-. Thus, the concentration of Cl^- on the steel surface decreased, and the corrosion reaction was suppressed. The total curve moved to the positive direction with the addition of the inhibitor. All

these results suggested that Na_2WO_4 reduced anodic dissolution greatly, and it served as an anodic inhibitor in seawater [29]. Considering the cost and inhibition effect, 1.0 g/L was chosen for the next experiment. From Fig. 1b, after adding $ZnSO_4$ to the seawater that contained 1.0 g/L Na_2WO_4, the polarization curves move to the negative direction a little, but they were still on the positive side compared to the blank one. Besides, the shapes of the curves were similar to those in Fig. 1a. Correspondingly, the composite inhibitors also decreased the anodic reaction rate significantly. Generally, corrosion current density I_{corr} could reflect the reaction rate. The smaller the I_{corr} was, the slower the corrosion rate was. In terms of the lower part of Table 1, we concluded that Na_2WO_4 and $ZnSO_4$ had synergistic effect on the inhibition of mild steel in natural seawater, and the Zn^{2+} acted as synergist, which could form coordination complexes with Na_2WO_4 so that to enhance the inhibition effect [30]. Therefore, the combination of 1.0 g/L Na_2WO_4 and 0.3 g/L $ZnSO_4$ was chosen for wet/dry tests.

Table 1. Corrosion parameters for mild steel in seawater in the absence and presence of different concentrations of inhibitors.

Inhibitor	C (g/L)	E_{corr} (mV *vs.*SCE)	I_{corr}	β_c (mV/dec)	β_a (mV/dec)
	x = 0.0	–667	8.56	589.9	65.9
	x = 0.1	–611	4.02	107.2	102.8
x g/L Na_2WO_4	x = 0.5	–529	2.58	175.6	110.3
	x = 1.0	–480	1.63	107.5	90.4
	x = 1.5	–422	2.46	148.5	85.4
1.0 g/L Na_2WO_4 + y g/L $ZnSO_4$	y = 0.1	–529	2.11	104.3	120.6
	y = 0.2	–531	1.60	96.1	113.8
	y = 0.3	–527	0.10	155.2	119.7
	y = 0.4	–515	0.79	151.0	76.8

3.1.2. EIS

Figure 2a presents the Nyquist plots of mild steel in seawater that contained different concentration of Na_2WO_4, in which all impedance spectra exhibited a single depressed semicircle, indicating that the addition of sodium tungstate didn't change the corrosion mechanism [31]. Therefore, the EIS results were simulated using a simple equivalent circuit containing a solution resistance R_s, a charge transfer resistance R_{ct} and a constant phase element CPE_{dl}, as shown in Fig. 3. We used CPE_{dl} instead of capacity cell in order to obtain more accurate results. In addition, the definition of a CPE_{dl} was expressed as [32, 33]:

$$Z = \frac{1}{Y_0 \left(j2\pi f \right)^n} \quad (1)$$

where Y_0 was a proportional factor, j was the imaginary root, f was the frequency of AC signal, and n was the deviation parameter.

The fitted parameters are listed in the upper part of Table 2. In generally, the capacitive semicircle at high frequencies which was caused by the charge transfer resistance and double layer capacitance usually represented the response of a surface film [34, 35]. Fig. 2 shows that after adding Na_2WO_4, the capacitive reactance arc radius increased, which suggested that Na_2WO_4 decreased the rate of corrosion reaction. Besides, the value of charge transfer resistance R_{ct} could reflect the corrosion rate of mild steel. When the value of R_{ct} was greater, the corrosion rate was smaller. Correspondingly, the inhibition effect was better. Considering from the diagram and parameters, 1.0 g/L was chosen for the next experiment.

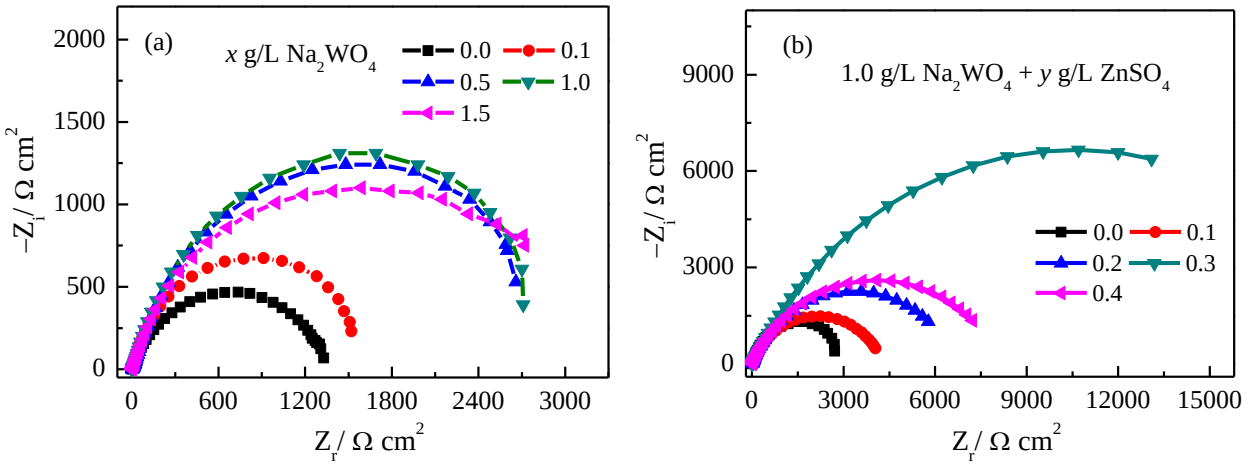

Figure 2. Nyquist plots of mild steel in seawater with (a) x (x = 0~1.5) g/L Na_2WO_4 and (b) 1.0 g/L Na_2WO_4 + y (y = 0~0.4) g/L $ZnSO_4$.

Fig. 2b exhibited the Nyquist plots of mild steel in seawater that contained 1.0 g/L Na_2WO_4 and different concentrations of $ZnSO_4$. It can be obtained that the addition of $ZnSO_4$ vastly increased the capacitive reactance arc radius and didn't alter the profile of the impedance behaviour [36], indicating that two compounds acted synergistically for the inhibition of mild steel corrosion. The equivalent circuit is shown in Fig. 3. The fitted parameters were displayed in the lower part of Table 2. On the basis of Fig. 2b and Table 2, 1.0 g/L Na_2WO_4 and 0.3 g/L $ZnSO_4$ were the best combination for wet/dry cyclic experiments, which was in accordance with the results of polarization measurements.

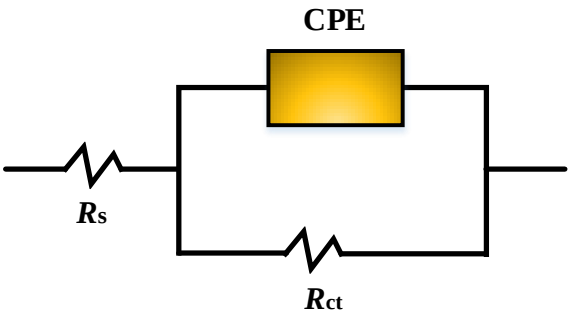

Figure 3. Equivalent circuit model used to fit the EIS experiment data.

Table 2. Fitted EIS parameters for mild steel in seawater with and without different concentrations of inhibitors.

Inhibitor	C (g/L)	R_s (Ω cm^2)	CPE$_{dl}$		R_{ct} (Ω cm^2)
			$C_{dl} \times 10^4$/(μF cm^{-2})	n	
x g/L Na_2WO_4	x = 0.0	1.72	3.31	0.82	1293
	x = 0.1	2.74	6.02	0.80	1740
	x = 0.5	2.07	8.69	0.76	3779
	x = 1.0	3.33	8.35	0.73	3916
	x = 1.5	1.15	8.70	0.70	3734
1.0 g/L Na_2WO_4 + y g/L $ZnSO_4$	y = 0.1	4.54	2.63	0.77	4296
	y = 0.2	2.26	3.25	0.75	6701
	y = 0.3	2.68	2.40	0.72	21160
	y = 0.4	1.40	2.02	0.72	8210

3.2 Wet/dry experiments results

3.2.1. Polarization measurements

Fig. 4 shows the polarization curves of mild steel after 10 cycles in seawater with and without STZS. Electrochemical corrosion kinetics parameters such as I_{corr}, E_{corr}, β_a, and β_c, which were obtained by extrapolation of the anodic and cathodic regions of the Tafel plots were listed in Table 3. Besides, inhibition efficiency η_p was calculated by the equation as follows:

$$\eta_p(\%) = \frac{I_{corr}^0 - I_{corr}}{I_{corr}^0} \times 100 \qquad (2)$$

where I_{corr}^0 and I_{corr} acted as the corrosion current density in the absence and presence of STZS, respectively.

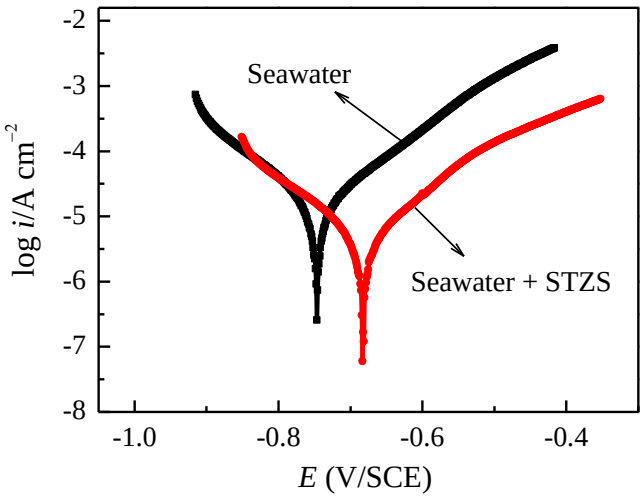

Figure 4. Polarization curves of mild steel in seawater in the absence and presence of STZS after 10 wet/dry cycles.

It could be observed from Fig. 4 that the curve in the presence of STZS moved to the positive direction for about 70 mV when compared to the blank one, and the anodic reaction was suppressed a lot. This phenomenon indicated that STZS could be classified as a mixed-type inhibitor that mainly inhibited the anodic reaction [37]. The parallel anodic curves suggested that the anodic reaction mechanism didn't change with the addition of STZS. The two cathodic curves coincided with each other suggesting that the STZS didn't influence the mechanism of the uptake of O_2, but restrained the rate of charge transferring. Table 3 showed that the current density I_{corr} decreased from 19.03 μA/cm^2 to 2.89 μA/cm^2, and η_p obtained by Eq. (2) could reach to a quite high value of 84.81%, confirming that the composite inhibitors STZS could serve as high efficient inhibitor at splash zone and was a new choice to be applied in PTC technology.

Table 3. Parameters for mild steel in seawater with and without STZS after 10 wet/dry cycles.

Solution	E_{corr} (mV *vs.* SCE)	I_{corr} (μA/cm^2)	β_c (mV/dec)	β_a (mV/dec)	η_p
Seawater	−746	19.03	132.75	144.38	/
Seawater + STZS	−681	2.89	99.05	115.13	84.81%

3.2.2. EIS

Nyquist plots of the specimens in seawater in the absence and presence of STZS after different cycles are displayed in Fig. 5. As for Fig. 5a, it seemed that impedance spectroscopy almost were linear, and a Warburg impedance [38] appeared at low-frequency, indicating that diffusion process was the rate determining step and corrosion products increased constantly on the work electrode surface. The electrode reaction was fast, and Fe^{2+} was consumed quickly at the electrode surface, while the concentration of Fe^{2+} in bulk solution was bigger contrast, thus caused the presence of Warburg impedance. With the time going on, the slope of the "line" decreased, suggesting that the corrosion products film can't protect the substrate from the further corrosion in seawater, and more serious corrosion happened as time goes on. While for the impedance spectroscopy that with STZS (as shown in Fig. 5b), depressed semicircles were obtained after different cycles. The phenomenon indicated that the addition of SZTS decreased the dispersion effect, which is due to the more uniform deposition on the cathode surface. The capacitive reactance arc at high-frequency was caused by double-layer capacity and charge transfer resistance [39]. While at low-frequency, the Warburg impedance disappeared, instead, a capacitive reactance arc appeared which related to the products film that prevented the further corrosion reaction [40]. The phenomenon was different from that in atmosphere corrosion or the total immersion corrosion [41, 42].

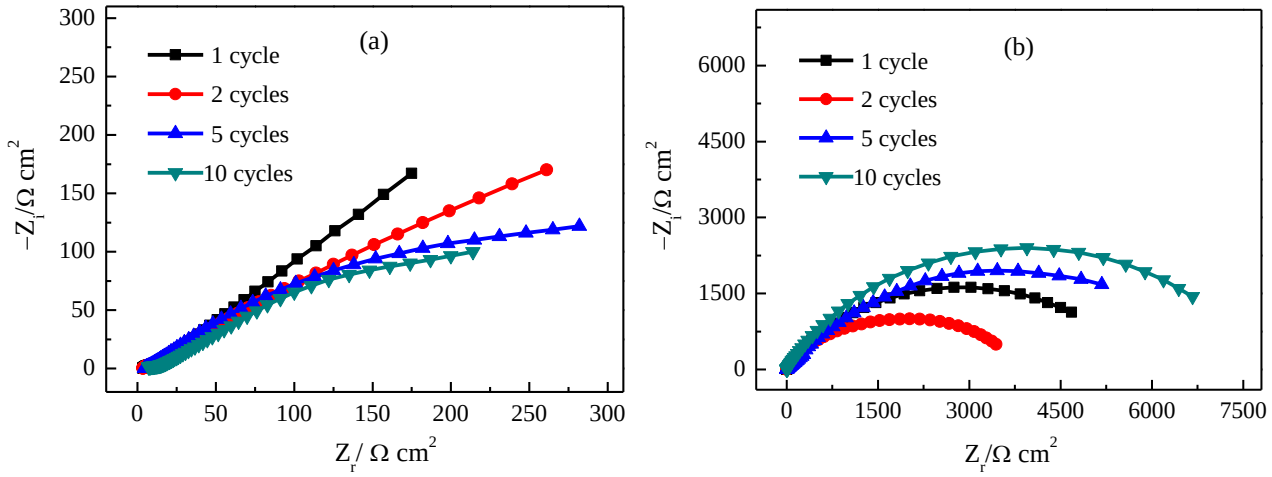

Figure 5. Nyquist plots of mild steel in seawater in the absence (a) and presence (b) of STZS for different cycles.

The equivalent circuits employed for the system are presented in Fig. 6. For both of the models, the resistance R_s was the resistance of the solution, R_{ct} reflected the charge transfer resistance, CPE_{dl} was the double-layer capacitance, R_{cp} was electrode surface film resistance, Q_{cp} was electrode surface film capacitor, and n was error parameter (determined by the surface morphology) [43]. Z_w in Fig. 6a represented Warburg impedance. The fit parameters of two systems were listed in Table 4. According to the data, we obtained that as time went on, the value of R_{ct} in seawater decreased first, then increased a little after a fall. On the whole, R_{ct} remained a low value all the time, indicating that the product film formed on the steel surface in seawater could not prevent waves destroying the steel substrate. For the R_{ct} in seawater that containing STZS, at initial stage of immersion, it kept a high value. After two cycles, it decreased a little due to the happen of corrosion reaction. Afterwards, when five cycles passed away, it rose again because of the formation of the more stable surface film, which guarded against the impact of ocean waves. Therefore, after ten cycles, the value of R_{ct} still remained high, as we expected.

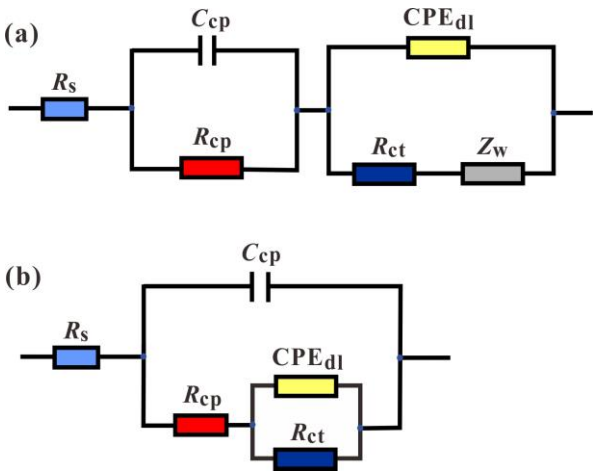

Figure 6. Equivalent circuit models used to fit the EIS experiment data of specimens in the absence (a) and presence (b) of STZS.

Table 4. Fitted parameters for mild steel in seawater in the absence and presence (values in brackets) of STZS for different cycles.

cycles	R_s (Ω cm^2)	C_{cp} (μF cm^{-2})	R_{cp} (Ω cm^2)	CPE_{dl}		R_{ct} (Ω cm^2)	Z_w (Ω^{-1} cm^{-2} $s^{0.5}10^{-3}$)
				Y_0/(μF cm^{-2})	n		
1	3.37 (1.70)	2774 (11.9)	3.54 (0.38)	821 (337)	0.71 (0.63)	7.88 (5965)	16.6
2	4.41 (2.32)	134.4 (1.07)	2.34 (2.38)	2996 (227)	0.78 (0.69)	4.16 (3450)	63.0
5	3.06 (1.83)	469.2 (1.93)	7.10 (4.23)	2803 (419)	0.78 (0.52)	18.25 (6359)	18.8
10	2.36 (1.45)	6948 (2.81)	36.68 (3.57)	6948 (245)	0.75 (0.69)	21.94 (8077)	5.9

3.2.3. Weight loss tests and surface analysis

The average weight loss of the mild steel samples in seawater with and without STZS was determined after 10 cycles at 298 K to examine whether the composite inhibitors was efficient for steel under wet/dry cyclic condition or not. The corrosion rate v (mg cm^{-2} h^{-1}) and inhibition efficiency η_w were evaluated by the following formulas [44]:

$$v = \frac{\Delta W}{S \cdot t} \quad (3)$$

$$\eta_w(\%) = \frac{v_0 - v_i}{v_0} \times 100 \quad (4)$$

where ΔW was the average weight loss (mg), S was the surface area of specimens (cm^2), t was the experiment time (d), v_0 and v_i signified the corrosion rate in the absence and presence of STZS, respectively.

According to Table 5, corrosion rate v decreased sharply with the addition of STZS, suggesting that STZS had excellent inhibition effect at the wet/dry cyclic condition, and a high η_w of 80.9% was achieved after 10 cycles.

Table 5. Weight loss results of mild steel in seawater in the absence and presence of STZS after 10 cycles.

Solution	ΔW (mg)	S (cm^2)	v (mg cm^{-2} d^{-1})	η_w
Seawater	306.6	26.62	1.15	/
Seawater + STZS	60.2	26.81	0.22	80.9%

Recognizing a problem is the first step in finding a solution. So unremitting efforts were made to explain the corrosion inhibition mechanism. SEM photographs obtained from mild steel surface before and after 10 cycles in seawater in the absence and presence of STZS are shown in Fig. 7. Compared with the specimen before immersion (Fig.7a), the surface after 10 cycles were strongly

corroded. For Fig.7b, rusty scale was sags and crests, which included the upper one and the lower one. Granulate and spongy substances coexisted in the rust, which morphology was rather tanglesome. The loose surface made it easy for corrosive liquid and O_2 to transfer, thus corrosion happened continually. On the contrary, For Fig.7c, rusty scale was uniform with small embossing on the surface. The compact surface film could resist the further corrosion. Judging from the morphology after treating by two different conditions, we concluded that STZS served as a favourable inhibitor in wet/dry cyclic condition.

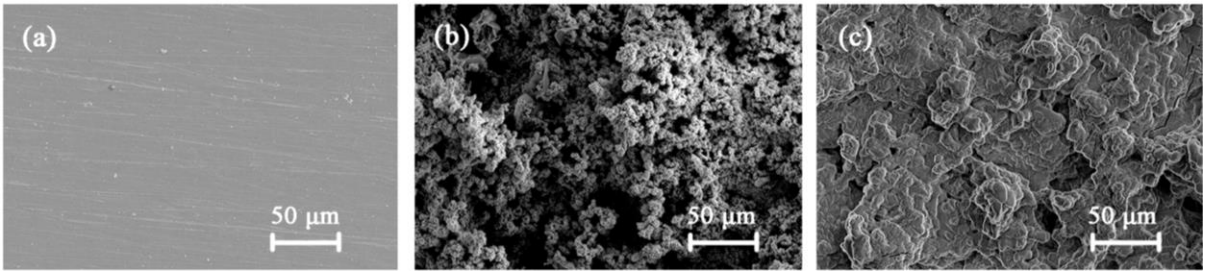

Figure 7. SEM photographs of mild steel surface before (a), and after 10 cycles in seawater in the absence (b) and presence (c) of STZS.

X-ray diffraction (XRD) analyses were used to identify the chemical composition of the rusty scale. The XRD spectrums of the specimens after 10 cycles in seawater without and with STZS are shown in Fig. 8. For Fig. 8a, the mainly substances were Fe_3O_4 and FeOOH, while in Fig. 8b, the products were most Fe_2WO_6 and $Zn(OH)_2$.

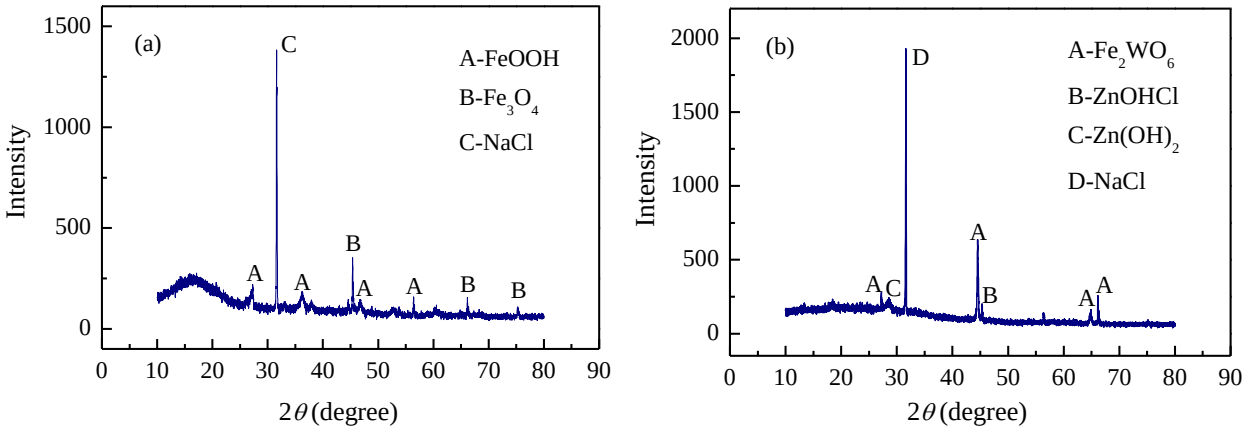

Figure 8. XRD spectrums of the products after 10 cycles in seawater without (a) and with (b) STZS.

3.3. Corrosion behaviours and inhibitor effects under different wet/dry ratios

Further study about the mild steel corrosion behaviours and the inhibitor effects under different wet/dry ratios were investigated by electrochemical methods. Fig. 9 gives the polarization curves in the absence and presence of STZS. The electrochemical parameters are presented in Table 6. The data

gathered in the study suggested that the corrosion density I_{corr} varied with the change of wet/dry ratios. In concrete terms, the values of I_{corr} decreased when the drying time increased in each cycle.

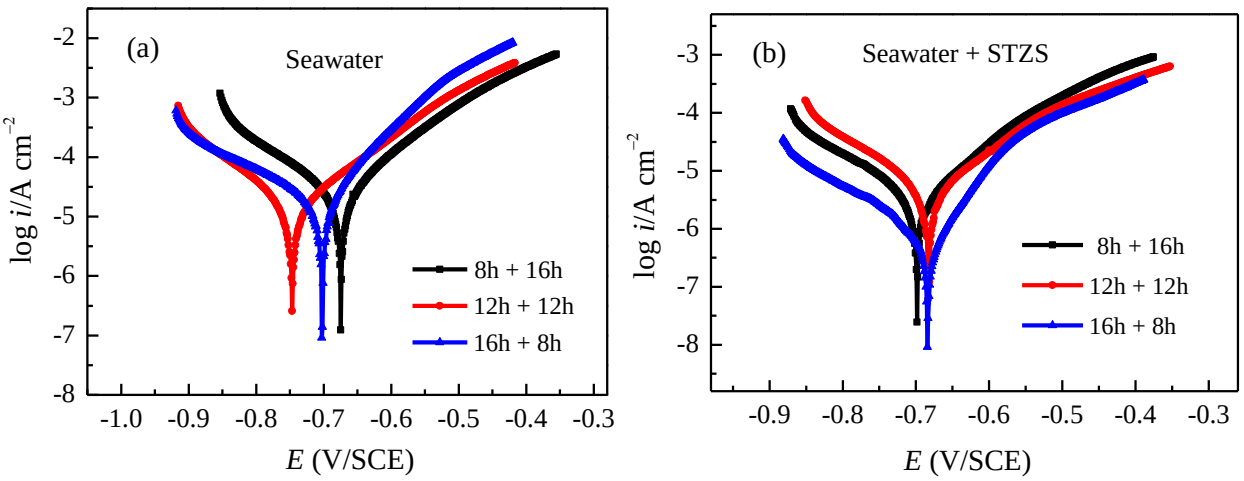

Figure 9. Polarization curves of mild steel in seawater in the absence (a) and presence (b) of STZS after 10 cycles for different wet/dry ratios.

Table 6. Electrochemical parameters for mild steel in seawater without and with (values in brackets) STZS after 10 cycles under different wet/dry ratios.

Ratios	E_{corr} (mV *vs.* SCE)	I_{corr} (μA/cm^2)	β_c (mV/dec)	β_a (mV/dec)
8h + 16h	−674 (−698)	29.26 (4.50)	153.38 (149.70)	120.36 (125.80)
12h + 12h	−746 (−681)	19.03 (2.89)	132.75 (99.05)	144.38 (115.13)
16h + 8h	−703 (−683)	10.48 (0.89)	169.54 (142.34)	97.88 (79.92)

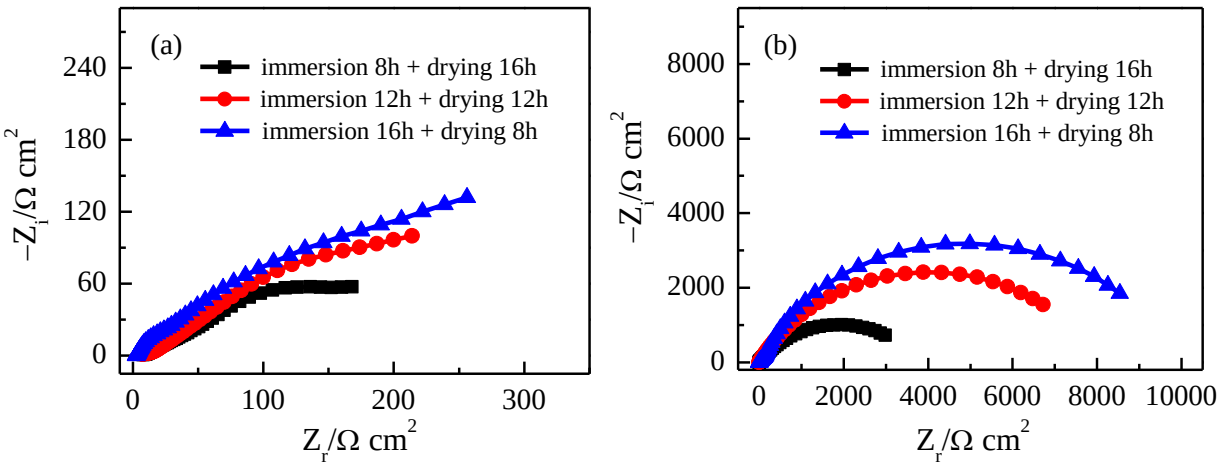

Figure 10. Nyquist plots of mild steel in seawater in the absence(a) and presence(b) of STZS after 10 cycles for different wet/dry ratios.

Fig.10 shows the Nyquist plots of mild steel in seawater in the absence and presence of STZS after 10 cycles under different wet/dry ratios. Table 7 lists the fitting data using the equivalent circuit

in Fig. 6. All of the conditions were same for the three groups of experiments except the wet/dry ratio. From the pictures and data, we obtained that the larger the wet/dry ratio was, the higher the R_{ct} value was. In other words, corrosion was severer as the drying time increased for one cycle. When steel was in wet/dry cycle state, the interaction of electrode depolarization effect at dry environment and the polarization effect at wet environment accelerated the corrosion rate, which led to corrosion reaction at wet/dry cycle zones was more serious than that at full immersion zone. What's more, the liquid membrane layer at metal surface became thinner and chloride concentration increased during the drying process. Therefore, the permeation rate of aggressive Cl^- was accelerated [45]. Besides, oxygen was much easier to diffuse into the interface of electrolyte and metal, which improved the cathodic reduction process [46]. The longer the drying time was, the bigger Cl^- permeate rate was, and the severer the corrosion was, as the experiments results showed.

Table 7. Fitted parameters for mild steel in seawater without and with (values in brackets) after 10 cycles of different wet/dry ratios.

Ratios	R_s (Ω cm^2)	C_{cp} (μF cm^{-2})	R_{cp} (Ω cm^2)	CPE_{dl}		R_{ct} (Ω cm^2)	Z_w (Ω^{-1} cm^{-2} $s^{0.5}$ 10^{-3})
				Y_0/(μF cm^{-2})	n		
8h + 16h	3.95 (1.24)	8630 (0.88)	40.10 (2.55)	1234 (520)	0.61 (0.62)	14.88 (3778)	2.51
12h + 12h	2.36 (1.44)	6948 (2.81)	36.68 (3.57)	6948 (245)	0.75 (0.68)	21.94 (8068)	5.92
16h + 8h	2.58 (4.32)	15450 (8.17)	10.41 (45.46)	3389 (207)	0.62 (0.70)	310 (9460)	8.16

3.4. Mechanism of corrosion inhibition

In order to explain all the experimental results, a plausible mechanism of corrosion inhibition is proposed as shown in Fig. 11.

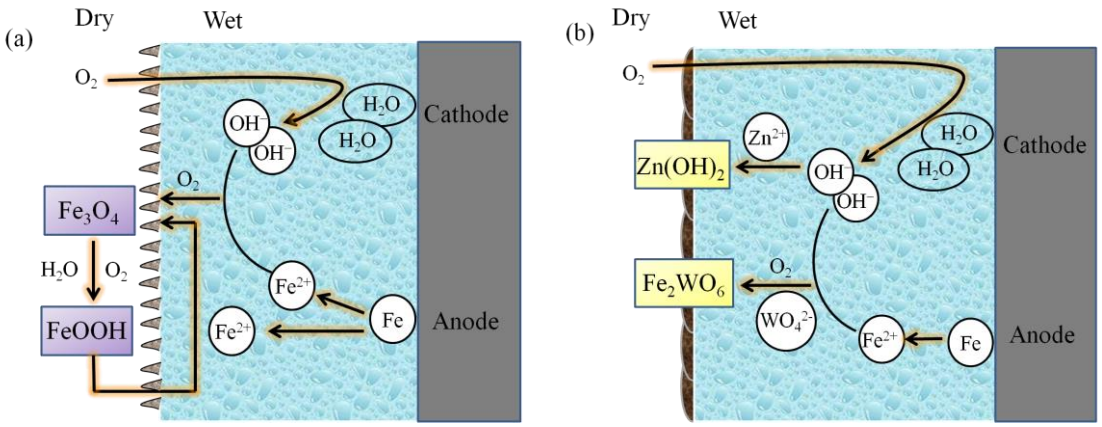

Figure 11. Proposed schematic for the corrosion mechanism under wet/dry cyclic condition tests in seawater without (a) and with (b) STZS.

In a word, the corrosion of mild steel in seawater wet/dry condition was the continuous formation of Fe_3O_4 and FeOOH, and the transition between the two substances. The rust itself acted as catalysts and took part in the electrochemical reaction, which accelerated the corrosion process [47]. With time going on, the specimens were damaged continually.

For seawater containing STZS medium in the wet condition, due to the existence of Zn^{2+}, then the following reaction was easier:

$$Zn^{2+} + 2OH^- \rightarrow Zn(OH)_2 \quad (5)$$

The reaction above hindered the reaction of Fe^{2+} combined with OH^-, then decreased the dissolution of Fe indirectly. In chloride-containing solutions, the Cl^- anions might react with $Zn(OH)_2$ to form soluble $[Zn^{2+}Cl^-OH^-]$ complex [48], as observed in XRD spectrums.

While in the dry condition, $Fe(OH)_2$ was oxidized by O_2:

$$4Fe(OH)_2 + O_2 + 2\,WO_4^{2-} \rightarrow 2Fe_2WO_6 + 2H_2O + 4OH^- \quad (6)$$

Then, the products attached to the electrode surface and hindered the corrosion reaction immensely. Therefore, these continuous precipitation reaction by ST and ZS can synergistically suppress corrosion of Fe in seawater wet/dry condition.

4. CONCLUSION

The desired concentrations (1.0 g/L Na_2WO_4 + 0.3 g/L $ZnSO_4$) of the composite inhibitors (STZS) were selected and it turned out that STZS showed excellent inhibition for mild steel in seawater wet/dry cyclic condition. Charge transfer resistance in EIS test remained stable after 5 cycles in the presence of STZS, revealing the durability of the STZS. The inhibition efficiency obtained from polarization measurements was 84.81% which is in good agreement with that obtained from weight loss tests (80.51%). For different wet/dry ratios, the longer the drying time was, the faster the reaction rate was. The corrosion of mild steel in seawater wet/dry condition was the continuous formation of Fe_3O_4 and FeOOH, and the transition between the two substances. While in seawater that contained the STZS, the formation of $Zn(OH)_2$ retarded the dissolution of iron and the products Fe_2WO_6 attached to the electrode surface and hindered the corrosion reaction.

References

1. F. Corvo, T. Perez, L.R. Dzib, Y. Martin, A. Castaneda, E. Gonzalez, J. Perez, *Corros. Sci.*, 50 (2008) 220-230.
2. M. Stipanicev, F. Turcu, L. Esnault, O. Rosas, R. Basseguy, M. Sztyler, I.B. Beech, *Bioelectrochemistry*, 97 (2014) 76-88.
3. P. Traverso, E. Canepa, *Ocean Eng*., 87 (2014) 10-15.
4. J. Zhang, C.X. Sun, Z.H. Yu, J.B. Cheng, W.Z. Li, J.Z. Duan, *Int. J. Electrochem. Sci*., 9 (2014) 5712-5721.
5. Y. Qiang, S.T. Zhang, S.Y. Xu, L. Guo, N.X. Chen, I.B. Obot, *Int. J. Electrochem. Sci*., 11 (2016) 3147-3163.
6. Y. Qiang, S. Zhang, S. Yan, X. Zou, S. Chen, *Corros. Sci*. 126 (2017) 295-304.
7. B.R. Hou, B. Xiang, J. Zhang, J.Z. Duan, *Mater. Corros*., 54 (2003) 697-702.
8. R.E. Melchers, R. Jeffrey, *Corros. Sci*., 65 (2012) 26-36.
9. H. Meng, X. Hu, A. Neville, *Wear*, 263 (2007) 355-362.

10. R. Jeffrey, R.E. Melchers, Corrosion of vertical mild steel strips in seawater, *Corros. Sci*., 51 (2009) 2291-2297.
11. Y.Z. Shi, E. Tada, A. Nishikata, *J. Electrochem. Soc*., 162 (2015) C135-C139.
12. W. Han, C. Pan, Z.Y. Wang, G.C. Yu, *Corros. Sci*., 88 (2014) 89-100.
13. A.W. Momber, P. Plagemann, V. Stenzel, *Renew. Energy*, 74 (2015) 606-617.
14. J.A. Jeong, C.K. Jin, *Sci. Adv. Mater*., 6 (2014) 2165-2170.
15. X.T. Wang, J.Z. Duan, J. Zhang, B.R. Hou, *Mater. Lett*., 62 (2008) 1291-1293.
16. K.M.A. Hossain, S.M. Easa, M. Lachemi, *Build. Environ*., 44 (2009) 713-722.
17. D.L. Leng, *Mater. Performance*, 39 (2000) 28-33.
18. B.R. Hou, J. Zhang, J.Z. Duan, Y. Li, J.L. Zhang, *Corros. Eng. Sci. Technol*., 38 (2003) 157-160.
19. K. Tachibana, Y. Morinaga, M. Matuzumi, *Corros. Sci.*, 49 (2007) 149-157.
20. H.B. Gao, Q. Chen, J. Wan, B.Y. Liu, Z.X. Wan, B.R. Hou, *China Coatings*, 28 (2013) 39-43.
21. M.C. Scholant, E.F. Coutinho, S.P. Dias, D.S. Azambuja, S.N. Silva, S.M. Tamborim, *Surf. Interf. Anal.*, 47 (2015) 192-197.
22. Q. Qu, L. Li, W. Bai, S. Jiang, Z.T. Ding, *Corros. Sci*., 51 (2009) 2423-2428.
23. S.M.A. Shibli, V.S. Saji, *Corros. Sci*., 47 (2005) 2213-2224.
24. G.N. Mu, X.H. Li, Q. Qu, J. Zhou, *Corros. Sci.*, 48 (2006) 445-459.
25. S.A. Kanimozhi, S. Rajendran, *Int. J. Electrochem. Sci*., 4 (2009) 353-368.
26. Q.J. Xu, G.D. Zhou, H.F. Wang, W.B. Cai, *Anti-Corros. Method. M*., 53 (2006) 207-211.
27. Y.J. Qiang, L. Guo, S.T. Zhang, W.P. Li, S.S. Yu, J.H. Tan, *Sci. Rep.*, 6 (2016) 33305.
28. L. Guo, G. Ye, I.B. Obot, X.H. Li, X. Shen, W. Shi, X. Zheng, *Int. J. Electrochem. Sci*., 12 (2017) 166-177.
29. H. Ashassi-Sorkhabi, M.R. Majidi, K. Seyyedi, *Appl. Surf. Sci*., 225 (2004) 176-185.
30. H.Q. Fan, S.Y. Li, Z.C. Zhao, H. Wang, Z.C. Shi, L. Zhang, *Corros. Sci*., 53 (2011) 4273-4281.
31. S. Hong, W. Chen, H.Q. Luo, N.B. Li, *Corros. Sci.*, 57 (2012) 270-278.
32. H.Y. Ma, S.H. Chen, B.S. Yin, S.Y. Zhao, X.Q. Liu, *Corros. Sci*., 45 (2003) 867-882.
33. Y. Qiang, S. Zhang, B. Tan, S. Chen, *Corros. Sci*., 133 (2018) 6-16.
34. H. Ashassi-Sorkhabi, N. Ghalebsaz-Jeddi, F. Hashemadeh, H. Jahani, *Electrochim. Acta*, 51 (2006) 3848-3854.
35. Y. Qiang, S. Zhang, L. Guo, X. Zheng, B. Xiang, S. Chen, *Corros. Sci*., 119 (2017) 68-78.
36. M.B. Radovanovic, M.M. Antonijevic, *J. Adhes. Sci. Technol.*, 31 (2017) 369-387.
37. P. Morales-Gil, G. Negron-Silva, M. Romero-Romo, C. Angeles-Chavez, M. Palomar-Pardave, *Electrochim. Acta*, 49 (2004) 4733-4741.
38. A.T. Lusk, G.K. Jennings, *Langmuir*, 17 (2001) 7830-7836.
39. W. Gou, C. Lai, Z. Xiang, *Int. J. Electrochem. Sci*., 11 (2017) 9983-9993.
40. C. Zhang, J.M. Zhao, *Int. J. Electrochem. Sci*., 10 (2017) 9161-9179.
41. C. Andrade, C. Alonso, J. Sarria, *Cem. Concr. Compos*., 24 (2002) 55-64.
42. P. Refait, M. Jeannin, R. Sabot, H. Antony, S. Pineau, *Corros. Sci*., 90 (2015) 375-382.
43. F.E.T. Heakal, M.M. Hefny, A.M.A. El-Tawab, *J. Alloys Compd*., 491 (2010) 636-642.
44. F.Y. Cui, L. Guo, S.T. Zhang, *Mater. Corros*., 65 (2014) 1194-1201.
45. A.P. Yadav, A. Nishikata, T. Tsuru, *Corros. Sci*., 46 (2004) 169-181.
46. J.G. Liu, Z.L. Li, Y.T. Li, B.R. Hou, *Int. J. Electrochem. Sci*., 9 (2014) 8175-8181.
47. U.R. Evans, C.A.J. Taylor, *Corros. Sci*., 12 (1972) 227-246.
48. H. Ashassi-Sorkhabi, E. Asghari, *J. Electrochem. Soc*., 159 (2012) 1-7.